Multiband theory for heavy-ion neutron-pair transfer among deformed Gd nuclei

S. Y. Chu, J. O. Rasmussen, and M. A. Stoyer*
Lawrence Berkeley National Laboratory, Berkeley, California 94720

L. F. Canto and R. Donangelo
Universidade Federal do Rio de Janeiro, C.P.68528, 21945 Rio de Janeiro, Rio de Janeiro, Brazil

P. Ring
Technische Universität München, D-85748 Garching, Germany
(Received 6 October 1994; revised manuscript received 26 May 1995)

In this paper our microscopic wave functions for Gd isotopes are applied to calculating neutron-pair transfer probabilities in heavy-ion collisions. The ~2600-term wave functions come from Hamiltonian matrix diagonalization of systems of 12 Nilsson neutron orbitals, nearly half-filled. We use the lowest five bands in initial and final nuclei and calculate transfer for all even spins from 0 through 30. Results for the sudden approximation (infinite moment-of-inertia) for neutron-pair extraction from ^{156}Gd by ^{58}Ni at near Coulomb barrier energy, and extraction by ^{206}Pb are shown. Next neutron-pair deposition by the Ni and Pb projectiles is calculated. Finally, a finite moment-of-inertia semiclassical calculation is formulated and performed on the ^{156}Gd + ^{206}Pb system for n-pair transfer in both directions. The results are compared with experimental results. It is clear that the inclusion of the additional bands above the lowest two is important. Theory and experiment agree qualitatively on the rise of population above the yrast line at higher spins.

PACS number(s): 21.10.Re, 21.60.Ev, 23.20.Lv, 25.70.Hi

I. INTRODUCTION

In another paper [1] we expanded and applied a large-matrix diagonalization approach to the microscopic structure of spheroidal Gd nuclei. Now we wish to apply these wave functions of good particle number and angular momentum to nuclear reactions amenable for study in modern large-multiplicity gamma detector arrays like GAMMASPHERE or EUROGAM.

Neutron-pair transfer reactions have attracted great interest over the years as a probe for the important pairing properties of nuclei. In particular, the ground-to-ground (p,t) and (t,p) cross sections of even-even nuclei show a large enhancement of order $(\Delta/G)^2$, where Δ is the gap parameter and G the pairing force strength. The fact that some transfer strength goes to excited states is often described in terms of a pairing vibrational strength. The (p,t) and (t,p) reactions have been important probes for the low-spin states. Shihab-Eldin *et al.* [2] have made a study of these reactions among 0^+ states of deformed rare-earth nuclei. They used a prototype model that laid the groundwork for the present study. This earlier work diagonalized Hamiltonian matrices of 126×126 using near half-filled sets of nine Nilsson orbitals about the Fermi energy. The appeal of pair transfer using heavier ions is the possibility of studying the pairing structure of higher spin states. The long-range Coulomb force in the heavy-ion collision excites the deformed collision partner ground rotational band, so that near closest approach, the neutron pair tunneling probes the structure of rotationally excited states. Indeed, it was hoped [3] that heavy-ion neutron-pair transfer could be a simple meter of the Coriolis antipairing effect, where the pairing correlation gradually decreases with increasing spin.

Egido and Rasmussen [4], using HFB/RPA wave functions, explored the patterns of heavy-ion neutron-pair transfer among spheroidal rare earths up to high spin. The decreasing transfer to yrast states with increasing spin could be seen, as could systematic occurrence of transfer strength to yrare near the band-crossing region.

Theoretical studies [5] uncovered a new complication (richness) to the process, whereby the ground-to-ground pair transfer matrix elements in many cases did not, as spin increased, monotonically tend toward zero but passed through zero and changed sign to negative. This behavior was found theoretically to be closely related to the sharp band crossing (backbending) phenomena associated with the spin-alignment of an $i_{13/2}$ neutron pair. Ideas emerged of a Berry-phase interference as reaction paths streamed around both sides of "diabolic" points, where the lowest energy sheets touched in the angular momentum vs particle-number plane. First theoretical calculations of cross sections indicated rather large effects depending on whether or not a diabolic point was between the A and $A+2$ nuclei involved in the reaction [6–8]. Later work [9, 10], including the two lowest (yrast and yrare) bands in the theory instead of just the lowest, showed the effect on cross sections to be less and the experimental measurement of this "nuclear SQUID ef-

*Present address: Lawrence Livermore National Laboratory, Livermore, CA 94551.

fect" to be more difficult. Whether inclusion of just two bands, an idealized aligned band and ground band, is adequate for the calculation, is to be addressed in this paper. The need for better description of several of the lowest rotational bands for these transfer studies inspired the HMD (Hamiltonian matrix diagonalization) calculations of $^{154-158}$Gd in Ref. [1]. The 2600-configuration microscopic wave functions of that work, augmented by HMD calculations on reaction partners, constitute the main input for the reaction calculations of this paper. For practical reasons of vanishingly small cross sections, neutron-pair transfer cannot be studied much below the Coulomb barrier, and the theorist is forced to deal with nuclear-optical-potential complications of the near-barrier data.

In Sec. II the matrix elements for two-neutron transfer are formulated, first by sudden approximation and then by a modified semiclassical time-dependent Schrödinger (SCTDS) method [11]. In Sec. III the transfer formalism is applied to two-neutron pickup and stripping reactions involving a ^{156}Gd target. We show examples for two different projectiles, ^{58}Ni and ^{206}Pb, both at near-barrier energies. The sudden approximation is appropriate for cases where the deformed nucleus rotates only slightly during the course of the collision. As applied here the sudden approximation is the same as the classical-limit S-matrix (CLSM) method [8]. The method has great simplicity and allows for intuitive pictures of collision paths at different orientations of the symmetry axis of the spheroidal partner. As we shall apply it, the electromagnetic ($E2$) interaction is distributed over the path as r^{-3}, but the neutron transfer is assumed to take place entirely at the closest approach. The sudden approximation is decreasingly applicable to heavier projectiles, such as Pb, since the Gd will appreciably rotate during the collision. Thus, we show in this paper in sudden approximation only the Ni on Gd, where the approximation should be quite good.

The modified SCTDS calculations are more computationally intensive and less intuitive, but they can be applied widely, including for the heaviest systems. Here we include also the nuclear optical potential effects, important at near-barrier energies of most transfer experiments. We also have the transfer process distributed along the path, rather than confining it to closest approach. In the limit of small rotational spacing the SCTDS calculations should agree with the sudden approximation, a limit we have found useful in checking the codes.

The calculation of two-neutron transfer in full rigor is a formidable challenge, even for light projectiles on spherical nuclei; thus, a wide range of approximations must be considered to make the calculation practical. We shall restrict ourselves to consideration of two-neutron transfer between heavy even-even nuclei in head-on collisions. Furthermore, we will not attempt to calculate absolute cross sections but only the relative cross sections among rotational states in the lowest five bands of the deformed partner. We are aware of, but will not consider, recoil corrections due to the change in masses of the collision partners after transfer. A useful review of two-nucleon transfer for (p,t) and (t,p) reaction was given by Towner and Hardy [12]. For a critical review and presentation of the two-nucleon transfer theory between heavy ions, one should consult the 1975 paper of Götz *et al.* [13].

We need for our calculations effective pair-transfer matrix elements from particular Nilsson levels in the deformed partner, taking into account only implicitly the sum over states in the spherical partner for the $1n$-transfer intermediate and the sum over pairing configuration admixtures in the initial and final even-n systems in the spherical partner. Von Oertzen and colleagues in a series of papers have nicely showed, especially in their study of two spherical partners, how multinucleon transfer probabilities have distance-of-closest approach dependences that generally go as the single nucleon transfer probability raised to the power of the number of nucleons transferred. However, they often find enhancement factors (EF), which they can relate to coherence effects from sums at $1n$, $2n$, ...,xn stages of the process [14–17].

In the literature, particularly in papers attempting to reproduce absolute pair transfer cross sections, there has been attention to the question of simultaneous vs sequential transfer for two-nucleon transfer processes [18, 19]. The most detailed work we have found deriving and testing an effective first-order pair-transfer matrix element, based on a microscopic description, is that of Lotti *et al.* [20]. See also Dasso *et al.* [21].

Let us make a few estimates of the time scales involved in the heavy-ion transfer we focus on in this paper, namely, the near-barrier ^{206}Pb + ^{156}Gd system. For a pure Coulomb potential at a touching distance of 16.26 fm (radius constant $r_0 = 1.44$ fm) the Coulomb barrier is 465.0 MeV. The repulsive Coulomb force at this touching distance is 28.6 MeV fm^{-1}. This force divided by the reduced mass gives the classical acceleration a of 3.092×10^{43} fm sec^{-2} ($= 3.43 \times 10^{-4} c^2$ fm^{-1}). For an average neutron binding energy of 7 MeV, the characteristic tunneling length x_t for a neutron will be 1.72 fm. We may thus estimate a characteristic time interval over which most transfer will take place. This time $t_{\rm tran}$ will be twice the time the collision system needs to move from closest approach to a distance 1.72 fm out. Assuming uniform acceleration a, $t_{\rm tran} = 6.67 \times 10^{-22}$ sec. The "Q window" is $\hbar$ divided by this time, or ≈ 1.0 MeV. (If we take into account the tail of the attractive nuclear potential at closest approach, which would lower the acceleration at the turning radius, the collision time for tunneling will increase and the Q window will narrow, going to very small values as the turning radius approaches the top of the barrier.)

The usual interpretation of the Q window is that the kinematics of the reaction will favor single-neutron transfer to states within the energy window (here $\approx$1.0 MeV) around the final state (or virtual state) with $Q = 0$. The Pb spherical partner ^{206}Pb is so close to the 126 closed shell that pair addition mainly involves $p_{1/2}$ orbital intermediates and the pair removal mainly $f_{5/2}$ and $p_{3/2}$ orbitals. For the pair removal reaction from ^{156}Gd the Q value is -0.87 MeV, and the single-neutron removal to the odd-A ground states is -1.80 MeV. Other intermediate $1n$-removal states have even more negative Q values, all of them larger than the Q window. Thus, it seems

justified to consider simultaneous transfer, with its simpler radial dependence, to be dominant. Since we do not purport to calculate absolute transfer cross sections, we need only be concerned that the dozen Nilsson neutron orbitals nearest the Fermi energy have nearly equal pair transfer probabilities when averaged over the spheroidal nuclear surface. That is, there should be strong damping of residual Brink rules for matching tangential velocities of transferred nucleons at the touching surfaces. This point needs further theoretical and experimental study, but our rough estimates of the angular window for neutron transfer in these heavy nuclei is that the Brink velocity rules would be strongly damped.

We will be numerically solving coupled time-dependent Schrödinger equations of Alder-Winther-deBoer type, and the space-time dependence of our transfer matrix elements will be of the first-order form of simultaneous pair transfer.

In taking the pair transfer operator as only creating (annihilating) pairs in given Nilsson orbitals we are following a traditional assumption in treating two-nucleon transfer involving spheroidal nuclei. We will go beyond most previous studies in that we will use not only the $L = 0$ part of the pair creation (annihilation) operator but also the $L = 2$ and $L = 4$ parts.

II. MATRIX ELEMENTS FOR TWO-NEUTRON TRANSFER

The formulation for pair addition and pair removal is very similar, and therefore only the derivation for the pair addition transfer process is shown in this paper. For clarity let the target be the deformed nucleus, and the projectile be the spherical partner, although experiments may be run inversely. Only head-on collisions are treated, and the excitation of the projectile and its internal microscopic structure is ignored. The origin of the laboratory coordinate system is at the center of the target nucleus, and the projectile trajectory is along the z axis to closest approach and then back along the z axis (i.e., 180° scattering). Let R be the distance between the two nuclear centers. Then $R\mathbf{z}$ is the location of the center of the projectile, where $\mathbf{z}$ is the unit vector along the z axis. For pair addition, the pair bound in the projectile potential well can be considered in Born approximation for the pair transfer reaction. Then, the transition matrix elements $M_{\rm tx}(R)$ can be approximated as follows:

$$M_{\rm tx}(R) = \langle\, \Psi_f^{\rm targ}(N+2) \mid \sum_{i=1,2} \mathbf{V}_i(\mathbf{r}_i - R\mathbf{z})\phi_p(\mathbf{r}_1 - R\mathbf{z})\phi_{\bar{p}}(\mathbf{r}_2 - R\mathbf{z}) \mid \Psi_i^{\rm targ}(N)\,\rangle, \tag{1}$$

where $\mathbf{V}_i$ is the nuclear potential of the projectile nucleus for particle i; ϕ_p and $\phi_{\bar{p}}$ denote the single-particle wave function and its time-reversed state bound in the projectile nucleus, and N is the initial particle number of the target. The brackets $\langle\ \rangle$ imply integration of $\mathbf{r}_1$ and $\mathbf{r}_2$ over all space, but since the square shell-model potential $\mathbf{V}_i$ vanishes unless both $\mathbf{r}_1$ and $\mathbf{r}_2$ lie within the spherical surface, the integral is only over the limited volume. Let us ignore the broken pair contributions in Eq. (1) because their transfer probabilities will not receive the coherent pairing force enhancement and should thus be less important in these calculations. Then, evaluation of $M_{\rm tx}$ reduces to the task of evaluating the overlap integral of the pair wave functions from the projectile and the target nucleus. First, rotate $\psi_{j\Omega}(\mathbf{r})$, the orbital wave function of target nucleus, from the body-fixed frame into the laboratory frame. This gives

$$\psi_{j\Omega}(\mathbf{r}) \approx \sqrt{\frac{2j+1}{2(2l+1)}}\,\Re_{Nl}(r)Y_{l0}(\hat{\mathbf{r}})\left[\mathcal{D}^j_{\frac{1}{2}\Omega}(\omega)\sigma_{\frac{1}{2}} + \mathcal{D}^j_{-\frac{1}{2}\Omega}(\omega)\sigma_{-\frac{1}{2}}\right] + \sum_{m\neq 0} Y_{lm}\cdots, \tag{2}$$

where $\sigma_{\frac{1}{2}}$ and $\sigma_{-\frac{1}{2}}$ are the up and down components of the spin vector. In Eq. (2), we do not include $m \neq 0$ components, since the small range of θ contributing to the integral makes $m \neq 0$ components negligible. Indeed, these components vanish for $j = 1/2$ bound states in the projectile. The $\Re_{Nl}(r)$ is the radial wave function, Y_{l0} a spherical harmonic, and $\mathcal{D}^j_{\pm\frac{1}{2}\Omega}(\omega)$ the symmetric top wave function of Eulerian angles ω. While Ω is a good quantum number for Nilsson orbitals, the j is only an approximate quantum number, as is well known. The quantum numbers N and l depend on j. In the subsequent derivation the Nilsson level will be labeled by $(j\Omega)$, since j and Ω are frequently needed in the expressions. Next we write the antisymmetric pair wave function in the laboratory frame as follows:

$$\begin{aligned}
\frac{1}{\sqrt{2}}\left[\psi_{j\Omega}(\mathbf{r}_1)\psi_{j\,-\Omega}(\mathbf{r}_2) - \psi_{j\Omega}(\mathbf{r}_2)\psi_{j\,-\Omega}(\mathbf{r}_1)\right] &= \Re_{Nl}(r_1)\Re_{Nl}(r_2)Y_{l0}(\hat{\mathbf{r}}_1)Y_{l0}(\hat{\mathbf{r}}_2)\frac{2j+1}{2l+1} \\
&\quad\times\frac{1}{2}\left[\mathcal{D}^j_{\frac{1}{2}\Omega}(\omega)\mathcal{D}^j_{-\frac{1}{2}\,-\Omega}(\omega) - \mathcal{D}^j_{\frac{1}{2}\,-\Omega}(\omega)\mathcal{D}^j_{-\frac{1}{2}\Omega}(\omega)\right]\times\text{S.F.} \\
&\quad+\sum_{m,m'\neq 0} Y_{lm}(\hat{\mathbf{r}}_1)Y_{lm'}(\hat{\mathbf{r}}_2)\cdots, \\
&= \Re_{Nl}(r_1)\Re_{Nl}(r_2)Y_{l0}(\hat{\mathbf{r}}_1)Y_{l0}(\hat{\mathbf{r}}_2)\frac{2j+1}{2l+1}\sum_{\lambda=0,2,4\cdots} \\
&\quad\times\left[(2\lambda+1)\begin{pmatrix} j & j & \lambda \\ \frac{1}{2} & -\frac{1}{2} & 0\end{pmatrix}\begin{pmatrix} j & j & \lambda \\ \Omega & -\Omega & 0\end{pmatrix}\mathcal{D}^\lambda_{00}(\omega)\right]\times\text{S.F.} \\
&\quad+\sum_{m,m'\neq 0} Y_{lm}(\hat{\mathbf{r}}_1)Y_{lm'}(\hat{\mathbf{r}}_2)\cdots,
\end{aligned} \tag{3}$$

where S.F. represents the normalized singlet spin function. Then the overlap function for the pair of $(j\Omega)$ level and the pair wave function of the projectile can be written as

$$M_{\rm tx}^{(j\Omega)}(R) = \frac{1}{\sqrt{2}}\langle\,[\psi_{j\Omega}(\mathbf{r}_1)\psi_{j\,-\Omega}(\mathbf{r}_2) - \psi_{j\Omega}(\mathbf{r}_2)\psi_{j\,-\Omega}(\mathbf{r}_1)]\sum_{i=1,2}\mathbf{V}_i(\mathbf{r}_i - R\mathbf{z})\phi_p(\mathbf{r}_1 - R\mathbf{z})\phi_{\bar{p}}(\mathbf{r}_2 - R\mathbf{z})\,\rangle$$
$$= v_0\chi^2_{(j\Omega)}(R)\sum_{\lambda=0,2,4\cdots} T_\lambda^{(j\Omega)}\mathcal{D}^\lambda_{00}(\omega)\,, \tag{4}$$

where $T_\lambda^{(j\Omega)}$ and $\chi_{(j\Omega)}(R)$ are defined as follows:

$$T_\lambda^{(j\Omega)} = (2\lambda+1)(2j+1)\begin{pmatrix} j & j & \lambda \\ \frac{1}{2} & -\frac{1}{2} & 0\end{pmatrix}\begin{pmatrix} j & j & \lambda \\ \Omega & -\Omega & 0\end{pmatrix}\,, \tag{5}$$

$$\chi_{(j\Omega)}(R) = \sqrt{\frac{2l'+1}{4}}\int_{\theta_s=0}^{\theta_s=\pi}\int_{r_s=0}^{r_s=r_{\rm proj}} \Re_{Nl}(r)\Re^{\rm proj}_{N'l'}(r_s)P_{l'}(\cos\theta_s)P_l(\cos\theta)\,\sin\theta_s\,d\theta_s r_s^2\,dr_s, \tag{6}$$

where $r = \sqrt{r_s^2 + R^2 - 2r_sR\cos\theta_s}$, $\theta = \tan^{-1}[r_s\sin\theta_s/(R - r_s\cos\theta_s)]$, v_0 is the well depth for the projectile, r_s and θ_s are the coordinates centered at the spherical nucleus for integration, $r_{\rm proj}$ is the radius of the spherical nucleus, and N', l' are quantum numbers for the projectile single particle levels. Note that the integration for $\chi_{(j\Omega)}(R)$ is over the volume of the projectile. With all the pair overlap integrals calculated, the transfer operator can be defined:

$$\mathbf{V}_{\rm tx}(R) = \sum_{(j\Omega)} M_{\rm tx}^{(j\Omega)}(R)\mathbf{a}^\dagger_{j\Omega}\mathbf{a}^\dagger_{j\,-\Omega}$$
$$= v_0\sum_{(j\Omega)}\chi^2_{(j\Omega)}(R)\sum_\lambda T_\lambda^{(j\Omega)}\mathcal{D}^\lambda_{00}(\omega)\mathbf{a}^\dagger_{j\Omega}\mathbf{a}^\dagger_{j\Omega}$$
$$\times(-1)^{\frac{1}{2}-\Omega}\,. \tag{7}$$

Note that a time-reversal phase factor is inserted, since the time-reversed particle creation operator is used in the expression. The $\chi_{(j\Omega)}(R)$ can be expressed as a product:

$$\chi_{(j\Omega)}(R) = v_1\Re_{Nl}(R - r_{\rm proj})\,. \tag{8}$$

The factor v_1 has the dimensions of energy times volume, which we take to be an arbitrary parameter. Absorbed within v_1 are all of the spectroscopic factor complications of the spherical partner. The target radial wave function, $\Re_{Nl}$, decreases exponentially outside the nucleus; thus, the main contribution to the overlap integral comes from integrating near the surface of the projectile, namely at $R - r_{\rm proj}$. Most of the contributing orbitals $|\,Nlj\Omega\rangle$ will have similar neutron-pair separation energies. Thus, the wave function $\Re_{Nl}$ of the Nilsson orbital will here be replaced by an average s-wave, single-neutron wave function with asymptotic form

$$\Re(r) = C_{\rm norm}\exp[-\sqrt{2m_nE_{\rm bind}}\,r/\hbar]/r,$$

where m_n is the reduced neutron mass, $E_{\rm bind}$ is the neutron binding energy of the target, and $C_{\rm norm}$ is the normalization constant. Namely,

$$\chi_{(j\Omega)}(R) = \chi(R) = v_1\Re(R - r_{\rm proj})\,. \tag{9}$$

Then the two-neutron transfer operator can be written as follows:

$$\mathbf{V}_{\rm tx}(R) = v_0\chi^2(R)\sum_{(j\Omega)}\sum_\lambda T_\lambda^{(j\Omega)}\mathcal{D}^\lambda_{00}(\omega)\mathbf{a}^\dagger_{j\Omega}\mathbf{a}^\dagger_{j\Omega}(-1)^{\frac{1}{2}-\Omega}\,. \tag{10}$$

A. Sudden approximation

The wave function of the target nucleus comes from the Hamiltonian matrix diagonalization (HMD) calculations and can be expressed as follows:

$$|\,I\,M\,\alpha\,N\rangle = \mathcal{N}_I\sum_i \mathcal{D}^I_{MK_i}(\omega)\,b_i^N(I,\alpha)\,\varphi_i^N\,, \tag{11}$$

where the normalization constant $\mathcal{N}_I = \sqrt{I+\frac{1}{2}}/(2\pi)$, the φ_i^N is the basis configuration with the index i running over the various combinations of Nilsson orbital pair occupations. The $b_i^N(I,\alpha)$ is the corresponding amplitude of the eigenstate spin I, and band α. Here, the particle number N must be used to label the wave function, since we are dealing with wave functions of various particle number. Let us use the notation as in Eq. (11) to label the eigenstates. For head-on collisions the sudden approximation transfer amplitude from ground state $|\,0\,0\,0\,N\rangle$ to $|\,I\,0\,\alpha\,N{+}2\rangle$ is given by

$$\mathcal{A}_{0\,0\,N\to I\,\alpha\,N+2}$$
$$= \sum_{I_1,\alpha_1}\sum_{I_2,\alpha_2}\langle I\,0\,\alpha\,N{+}2\,|\,\mathcal{U}^\dagger\,|\,I_2\,0\,\alpha_2\,N{+}2\rangle\,\langle I_2\,0\,\alpha_2\,N{+}2\,|\,\mathbf{V}_{\rm tx}(R_0)\,|\,I_1\,0\,\alpha_1\,N\rangle\langle I_1\,0\,\alpha_1\,N\,|\,\mathcal{U}\,|\,0\,0\,0\,N\rangle\,. \tag{12}$$

The pair transfer is calculated only at closest approach, R_0. In head-on collisions, the quantum number M (spin projection on the z axis in the laboratroy frame) does not change, and since the ground state has $M=0$, M remains zero throughout the reaction. The operators $\mathcal{U}$ and $\mathcal{U}^\dagger$ represent the time propagator for incoming and outgoing paths. The time when the projectile is at closest approach, R_0 is defined as $t = 0$. Then $\mathcal{U}$ and $\mathcal{U}^\dagger$ take the form

$$\text{incoming}: \ \mathcal{U} = \exp\left(-\frac{i}{\hbar}\int_{-\infty}^{0} V(\omega, R(t))\, dt\right) , \tag{13}$$

$$\text{outgoing}: \ \mathcal{U}^\dagger = \exp\left(-\frac{i}{\hbar}\int_{0}^{\infty} V(\omega, R(t))\, dt\right) . \tag{14}$$

For the sudden approximation calculation, only the quadrupole Coulomb interaction is included, and the nuclear potential is ignored. The monopole interaction should be excluded from $V(\omega, R)$, since its effect is already taken into account in calculating the trajectory. So $V(\omega, R)$ can be written as

$$V(\omega, R) = \frac{Z_{\text{proj}} e^2 Q_2 \mathcal{D}^2_{00}(\omega)}{2R^3} , \tag{15}$$

where Q_2 is the quadrupole moment (in laboratory frame) of the deformed nucleus and Z_{proj} is the atomic number for the projectile. Furthermore, the time integration along the Rutherford trajectory can be carried out analytically as

$$-\frac{i}{\hbar}\int_{-\infty}^{0} V(\omega, R(t))dt = -i\frac{Z_{\text{proj}} Q_2 e^2}{6\hbar v_\infty a_0^2}\mathcal{D}^2_{00}(\omega) , \tag{16}$$

where a_0 is half the distance of closest approach and v_∞ is the velocity of the projectile at infinity. Let us express $\mathcal{U}$ and $\mathcal{U}^\dagger$ in terms of a multipole expansion as follows:

$$\mathcal{U} = \mathcal{U}^\dagger = \sum_\lambda \mathbf{Z}_\lambda \mathcal{D}^\lambda_{00}(\omega) , \tag{17}$$

with the coefficient $\mathbf{Z}_\lambda$ simply

$$\mathbf{Z}_\lambda = \frac{2\lambda+1}{8\pi^2}\int \mathcal{D}^\lambda_{00}(\omega)\, \exp\left[-\frac{i}{\hbar}\frac{Z_{\text{proj}} Q_2 e^2}{6v_\infty a_0^2}\mathcal{D}^2_{00}(\omega)\right] d\omega . \tag{18}$$

The matrices $\mathbf{X}$, $\mathbf{Y}$, and $\mathbf{Z}$ are defined slightly differently in Ref. [22]. They have no relation to spherical harmonics Y_{lm} nor to charge Z.

For clarity the integral in each of the three steps in Eq. (12) is shown separately as follows.

(i) Incoming path:

$$\begin{aligned}\langle I_1\, 0\, \alpha_1\, N \mid \mathcal{U} \mid 0\, 0\, 0\, N\rangle &= \mathcal{N}_{I_1}\mathcal{N}_0 \sum_i \left[\int \mathcal{D}^{I_1}_{0K_i}{}^*(\omega)\, \mathcal{D}^0_{0K_i}(\omega) \sum_\lambda \mathbf{Z}_\lambda \mathcal{D}^\lambda_{00}(\omega)\, d\omega\right] b_i^N(I_1, \alpha_1)\, b_i^N(0,0) \\ &= \sqrt{2I_1+1}\, \mathbf{Z}_{I_1}\, \mathbf{X}^N_{I_1}(0,0; I_1, \alpha_1),\end{aligned} \tag{19}$$

where $\mathbf{X}^N_\lambda(I_1, \alpha_1; I_2, \alpha_2)$ is the overlap integral for the intrinsic functions with the inelastic excitation of multipolarity λ:

$$\mathbf{X}^N_\lambda(I_1, \alpha_1; I_2, \alpha_2) \equiv \sum_K (-)^K \begin{pmatrix} I_1 & I_2 & \lambda \\ -0 & 0 & 0 \end{pmatrix}\begin{pmatrix} I_1 & I_2 & \lambda \\ -K & K & 0 \end{pmatrix} \sum_i b_i^N(I_1, \alpha_1)\, b_i^N(I_2, \alpha_2)\delta(K, K_i) . \tag{20}$$

(ii) Transfer at closest approach:

$$\begin{aligned}\langle I_2\, 0\, \alpha_2\, N{+}2 \mid \mathbf{V}_{\text{tx}}(R_0) \mid I_1\, 0\, \alpha_1\, N\rangle &= \mathcal{N}_{I_2}\mathcal{N}_{I_1} \sum_\lambda \sum_{i,i'} \left[\int \mathcal{D}^{I_2}_{0K_{i'}}{}^*(\omega)\, \mathcal{D}^\lambda_{00}(\omega)\, \mathcal{D}^{I_1}_{0K_i}(\omega)\, d\omega\right] \\ &\quad \times b_{i'}^{N+2}(I_2, \alpha_2)\, b_i^N(I_1, \alpha_1) \sum_{(j\Omega)} v_0 \chi^2(R_0)\, T^{(j\Omega)}_\lambda \langle \varphi_{i'}^{N+2} \mid \mathbf{a}^\dagger_{j\Omega}\mathbf{a}^\dagger_{j\Omega} \mid \varphi_i^N\rangle (-1)^{\frac{1}{2}-\Omega} \\ &= v_0\chi^2(R_0)\sqrt{(2I_1+1)(2I_2+1)} \sum_\lambda \mathbf{Y}^{N\to N+2}_\lambda(I_1, \alpha_1; I_2, \alpha_2) ,\end{aligned} \tag{21}$$

where $\mathbf{Y}^{N\to N+2}_{\lambda K}(I_1, \alpha_1, I_2\alpha_2)$ is defined as the overlap integral of the pair transfer with multipolarity λ:

$$\begin{aligned}\mathbf{Y}^{N\to N+2}_\lambda(I_1, \alpha_1; I_2, \alpha_2) &\equiv \sum_K (-)^K \begin{pmatrix} I_1 & I_2 & \lambda \\ -0 & 0 & 0 \end{pmatrix}\begin{pmatrix} I_1 & I_2 & \lambda \\ -K & K & 0 \end{pmatrix} \sum_{i,i'} b_{i'}^{N+2}(I_2, \alpha_2)\, b_i^N(I_1, \alpha_1)\, \delta(K, K_i) \\ &\quad \times \sum_{(j\Omega)} T^{(j\Omega)}_\lambda \langle \varphi_{i'}^{N+2} \mid \mathbf{a}^\dagger_{j\Omega}\, \mathbf{a}^\dagger_{j\Omega} \mid \varphi_i^N\rangle (-1)^{\frac{1}{2}-\Omega} .\end{aligned} \tag{22}$$

(iii) Outgoing path:

$$\begin{aligned}\langle I\, 0\, \alpha\, N{+}2 \mid \mathcal{U}^\dagger \mid I_2\, 0\, \alpha_2\, N{+}2\rangle &= \mathcal{N}_I\mathcal{N}_{I_2} \sum_i \left[\int \mathcal{D}^I_{0K_i}{}^*(\omega)\, \mathcal{D}^{I_2}_{0K_i}(\omega) \sum_\lambda \mathbf{Z}_\lambda \mathcal{D}^\lambda_{00}(\omega)\, d\omega\right] b_i^{N+2}(I, \alpha)\, b_i^{N+2}(I_2, \alpha_2) \\ &= \sqrt{(2I+1)(2I_2+1)} \sum_\lambda \mathbf{Z}_\lambda \mathbf{X}^{N+2}_\lambda(I_2, \alpha_2; I, \alpha) .\end{aligned} \tag{23}$$

Finally the transfer amplitude in Eq. (12) can be expressed simply as

$$\mathcal{A}_{0\,0\,N\to I\,\alpha\,N\pm2} = \chi(R_0)\sqrt{2I+1}\sum_{I_1,\alpha_1}(2I_1+1)\mathbf{Z}_{I_1}\mathbf{X}^N_{I_1}(0,0;I_1,\alpha_1)\sum_{I_2,\alpha_2}(2I_2+1)$$
$$\times\sum_{\lambda_2}\mathbf{Y}^{N\to N\pm2}_{\lambda_2}(I_1,\alpha_1;I_2,\alpha_2)\sum_{\lambda_3}\mathbf{Z}_{\lambda_3}\mathbf{X}^{N\pm2}_{\lambda_3}(I_2,\alpha_2;I,\alpha)\ . \tag{24}$$

B. Semiclassical time-dependent Schrödinger method

The treatment of the semiclassical time-dependent coupled Schrödinger equation (SCTDS) is well documented [23] but will be briefly discussed here so the relevant formulation can be introduced. The time-dependent Schrödinger equation is written as

$$i\hbar\frac{\partial}{\partial t}\,|\Psi(t)\rangle = \mathbf{H}(t)\,|\Psi(t)\rangle\ , \tag{25}$$

where

$$\mathbf{H}(t) = \mathbf{H}_0 + \mathbf{V}(t)\ , \tag{26}$$

where $\mathbf{H}_0$ is the Hamiltonian of the deformed target nucleus and $\mathbf{V}(t)$ is the interaction between target and spherical projectile. In this simple picture, the excitations of the spherical projectile are ignored. As discussed in Sec. II A, the monopole Coulomb interaction is used to calculate the classical Rutherford trajectory and should thus be excluded from $\mathbf{V}(t)$. Let us expand $\Psi(t)$ in terms of eigenstates of the target nucleus, namely

$$\Psi(t) = \sum_n a_n(t)\,|\,n\rangle e^{-iE_nt/\hbar}, \tag{27}$$

where $|\,n\rangle$ is the eigenstate of $\mathbf{H}_0$ and E_n is the corresponding eigenvalue. Then, we have a set of coupled differential equations:

$$i\hbar\dot{a}_n = \sum_m\langle n\,|\mathbf{V}(t)|\,m\rangle\exp[i(E_n-E_m)t/\hbar]\,a_m(t)\ . \tag{28}$$

The energy difference $(E_n - E_m)$ in Eq. (28) includes the reaction $Q_{\rm tx}$ value. These equations are solved with the initial condition at $t=-\infty$, where the projectile is far away and the target is entirely in the ground state, namely

$$a_n(-\infty) = \delta(0,n)\ . \tag{29}$$

Then, the final excitation amplitude is given by $a_n(\infty)$.

There is a standard method [11] to integrate Eq. (28). For our transfer calculation, however, the task is to calculate the matrix elements $\langle n\,|\mathbf{V}(t)|\,m\rangle$ using the microstructure wave functions. The perturbation $\mathbf{V}(t)$ in this case contains two terms, one for inelastic excitation and one for transfer:

$$\mathbf{V}(t) = V(\omega,R(t)) + \mathbf{V}_{\rm tx}(R(t))\ , \tag{30}$$

where $R(t)$ prescribes the Rutherford trajectory as a function of time. The evaluation of the matrix elements is similar to those shown in Sec. II A in sudden approximation.

For inelastic excitation. In this case, the particle number does not change, and the derivation is similar to Eq. (23), namely

$$\langle n\,|\,\mathbf{V}(t)\,|\,m\rangle = \langle I_2\,0\,\alpha_2\,N\,|\,\mathbf{V}(t)\,|\,I_1\,0\,\alpha_1\,N\rangle$$
$$= \sqrt{(2I_1+1)(2I_2+1)}\times\sum_{\lambda>0}\mathbf{Z}'_\lambda(t)\mathbf{X}^N_\lambda(I_1,\alpha_1;I_2,\alpha_2)\ , \tag{31}$$

where $\mathbf{Z}'_\lambda(t)$ is the λ multipole interaction when the projectile is at $R(t)$, as written below:

$$\mathbf{Z}'_\lambda = \frac{2\lambda+1}{8\pi^2}\int V(\omega,R(t))\mathcal{D}^\lambda_{00}(\omega)d\omega\ . \tag{32}$$

For transfer. Although the transfer is evaluated for the entire trajectory, it is significant only for distances near closest approach. In this case the particle number changes by two, and the derivation is similar to Eq. (21), namely

$$\langle n\,|\,\mathbf{V}(t)\,|\,m\rangle = \langle I_2\,0\,\alpha_2\,N+2\,|\,\mathbf{V}(t)\,|\,I_1\,0\,\alpha_1\,N\rangle$$
$$= v_0\chi^2(R(t))\sqrt{(2I_1+1)(2I_2+1)}\times\sum_\lambda\mathbf{Y}^{N\to N+2}_\lambda(I_1,\alpha_1;I_2,\alpha_2), \tag{33}$$

where the overlap $\chi(R(t))$ is evaluated when the projectile is at $R(t)$, as discussed in Eqs. (6) and (9).

III. NUMERICAL APPLICATION OF TRANSFER CALCULATIONS

First, we shall show the results of the pair transfer theory at various stages for the sudden approximation. In the sudden approximation of the classical limit S matrix (CLSM) the transfer reaction Q value, $Q_{\rm tx}$, is zero, all excited state energies are zero, and the transfer process takes place at the distance of closest approach. No nuclear optical potential is included, though it could be added. Three reactions on a ^{156}Gd target are shown in Figs. 1–3. The ^{58}Ni neutron-pair extraction is shown in Figs. 1. The ^{206}Pb n-pair extraction is shown in Figs. 2, and the ^{206}Pb n-pair deposition is shown in Figs. 3. The upper left figures (a) show the absolute value of the yrast rotational-state amplitudes at closest approach. In Fig. 1(a), for the Ni projectile, the most probable spin state is $6\hbar$, whereas in Fig. 2(a) and the identical Fig. 3(a) the most probable rotational state is spin $12\hbar$, with an appreciable amplitude tailing into the yrast-yrare band-crossing region around spin 16–18$\hbar$. (It was felt that the detection of Berry-phase interference associated with diabolic points where the spin-aligned band crosses the ground band might be possible with a Pb projectile, since the Coulomb excitation on the incoming path can pump

the rotational states up to the crossing region. From such considerations came the main motivation for the Oak Ridge experiments of Helmer *et al.* [24]). The usual interference oscillations are seen in the population pattern in yrast states, though we shall see that the effects of absorption by the imaginary optical potential damps the oscillations for near-barrier energies.

Examination of Figs. 1–3(b), which display in gray scale the population probabilities in various states at closest approach before transfer, shows the main population in the yrast band, but also some population in the higher bands, especially near the band-crossing spins 14–18$\hbar$. In the low-spin region, where the wave functions change only slowly with increasing spin, the orthogonality of states keeps the $M(E2)$ transition matrix elements small.

The lower left Figs. 1–3(c) show the probabilities in gray scale at closest approach, but after pair transfer. The energy levels in Figs. 1(c) and 2(c) now correspond to the final nucleus ^{154}Gd, with its sharp crossing of yrast and yrare. Neither of the two lowest bands beyond spin 18$\hbar$ show much population, though some goes into still higher bands. It was pointed out in the Ref. [1] that beyond spin 18$\hbar$ both the lowest two levels have strong neutron spin-alignment, and the extension of the ground band properties goes to higher levels. The soft-crossing ^{158}Gd final states are shown in Fig. 3(c). The energy-level and population patterns somewhat differ from Fig. 2(c) for ^{154}Gd. In both cases the transfer has spread the population into the higher bands also at low spins.

The lower right Figs. 1–3(d) show the populations after the collision partners have receded and further Coulomb excitation has taken place. This final stage pumps considerable population into the band-crossing region in the case of the Ni projectile Fig. 1(d), and it pumps population into very high spins for the Pb projectile Figs. 2(d) and 3(d). As earlier calculations of Canto *et al.* [6, 8] show, the sudden approximation result of this final stage in the Pb + rare-earth reaction is completely unrealistic. In the CLSM picture the nuclei in high-spin states over-rotate in the final stage, such that little change occurs due to Coulomb excitation in the final stage. The sudden-approximation final stage may be more realistic for the lower-Z nickel projectile. The best comparison to experiment for the higher-Z Pb projectile might be the populations after transfer but before the final stage of Coulomb excitation.

From a purely theoretical standpoint Figs. 2(d) and 3(d) are interesting in that the population pattern at highest spins may be an indication of the strength function of the extension of the less-aligned ground band. In ^{154}Gd the ground-band extension seems to center on the fourth band up, whereas in ^{158}Gd it is on the second

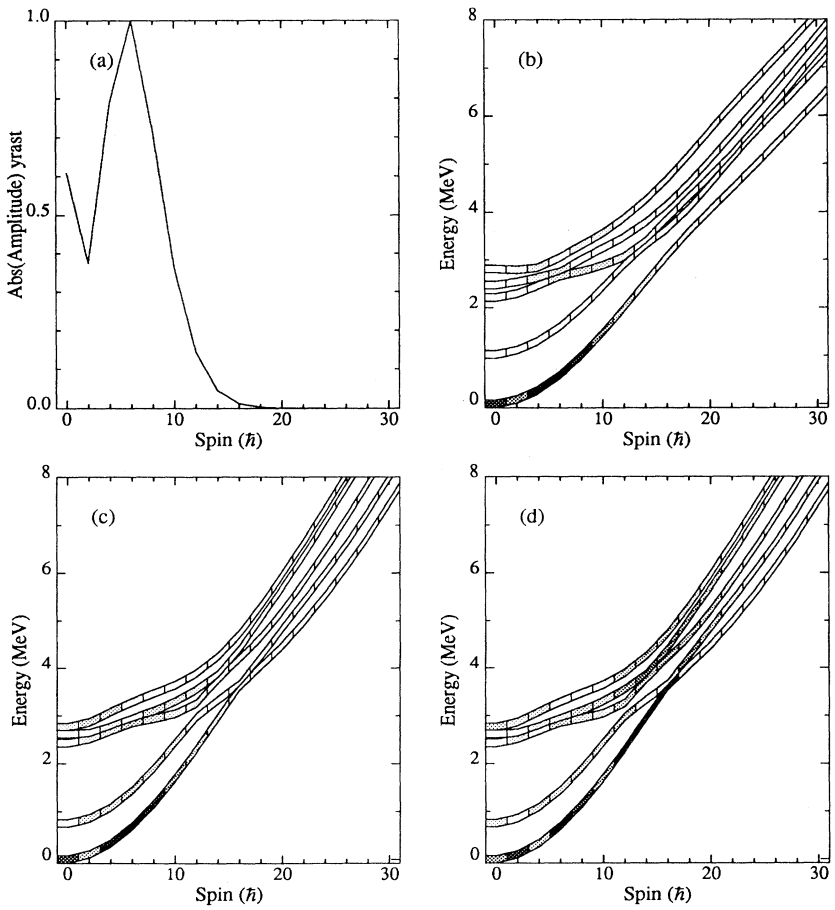

FIG. 1. Theoretical HMD sudden-approximation amplitudes in pair extraction transfer reaction ^{58}Ni+^{156}Gd $\rightarrow$ ^{60}Ni +^{154}Gd. (a) yrast bands and (b) all-band population in ^{156}Gd from Coulomb excitation at closest approach but before transfer. (c) population in ^{154}Gd at closest approach immediately after pair transfer, and (d) population in ^{154}Gd after collision partners have fully separated. The gray scale gives a semiquantitative overview of the transfer pattern. The gray-scale code is divided logarithmically, and the scale can be inferred from the yrast band of the upper right plot compared with the linear upper left plot, giving Coulomb excitation on the inward path.

(yrare) band. We shall discuss this further at the end of this paper.

To get a more realistic theory for high-Z projectiles like Pb, it is necessary to go beyond the sudden approximation, as in Refs. [9,10]. That is, use a modified semiclassical time-dependent perturbation theory in the rotational amplitudes. Such codes can take into account the energies of excited states and the $Q_{\rm tx}$ values for transfer reactions. To keep the number of rotational amplitudes from being too large, we restrict the calculation to head-on collisions, which means for the initial spin-zero collision partners only $M = 0$ amplitudes are considered.

We repeat the Gd+Pb cases previously shown in the sudden approximation. The neutron-pair transfer is not restricted to closest approach but spread over separation distance with an exponential falloff corresponding to the square of the one-neutron falloff. Since we are dealing with 5 bands, 16 spin states, and 2 nuclei, there are 160 coupled first-order differential equations in the sum of Eq. (28) to be integrated. In Refs. [9, 10] the $E2$ excitation and $L = 0$ transfer matrix elements were taken from a simple two-band mixing model of an idealized ground and neutron-spin-aligned band with constant mixing matrix element, $V_{\rm mix}$. The excitation matrix elements used now in this five-band calculation involve the overlap values of the approximately 2500 term configuration-mixed wave functions of the Hamiltonian matrix diagonalization (HMD) method discussed in Ref. [1]. The transfer matrix elements, as described in Eq. (33), involve a similar kind of operation of the pair creation (annihilation) operator summed over all the Nilsson orbitals. In this work we have extended the pair-transfer operator from the usual $L = 0$ to include also $L = 2$ and 4 transfer. To calculate nonzero L transfer without vast additional complication we need to associate j values with all neutron orbitals in the system. For this purpose we have assigned the dominant j value in the Nilsson orbital, rather than using j admixtures. Since in pair transfer there is a good deal of averaging over Nilsson orbitals near the Fermi energy, we believe the assignment of j values to orbitals for this purpose is justified.

Histograms of the final excitation amplitudes of various spin states in the five bands of ^{154}Gd, following the ^{206}Pb two-neutron stripping reaction, are shown in Fig. 4. These use the $\beta = 0.23$ basis wave functions from our earlier structure calculations [1]. We see, analogous to the sudden approximation results of Figs. 2(c,d), that the yrast band above the crossing (aligned band) gets almost no population. This illustrates a point made by Dasso and Winther [6] about transfer population avoiding the aligned band in sharp-crossing cases. As in the sudden case, there is appreciable population in the first three ex-

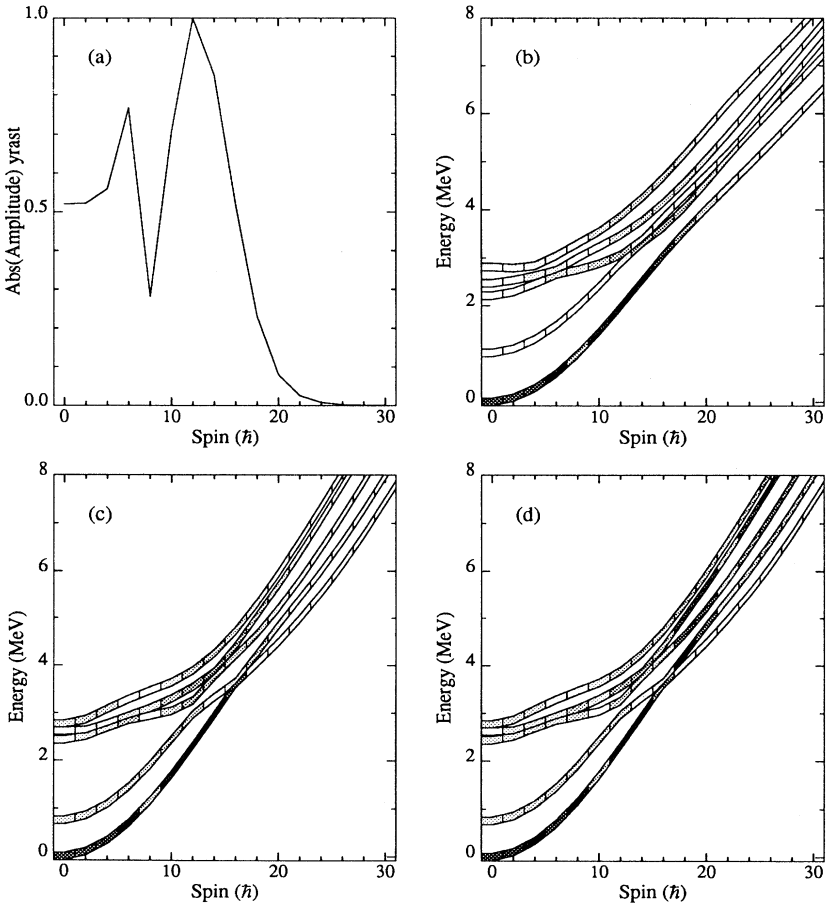

FIG. 2. Same as Fig. 1, but for ^{206}Pb projectile.

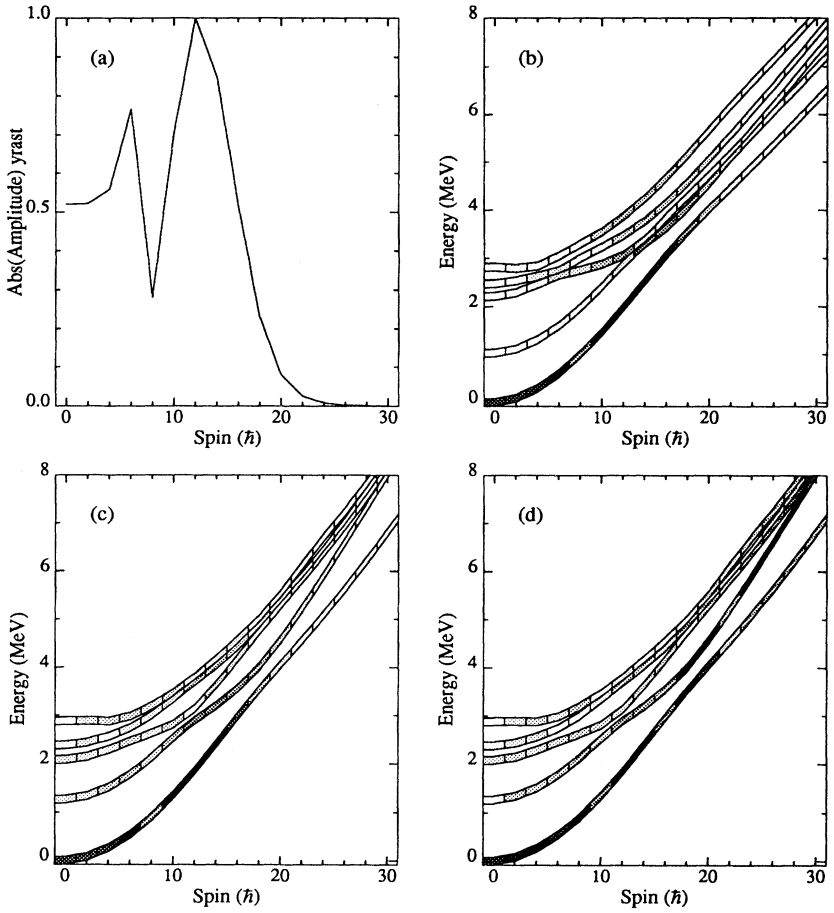

FIG. 3. Same as Fig. 2, but the transfer is pair deposition. Thus, (c) and (d) show ^{158}Gd population.

cited bands beyond the crossing spin of $18\hbar$. In Fig. 5 we show corresponding histograms for the ^{154}Gd, where the calculations used the larger deformation basis of $\beta = 0.28$. (We should note that these larger-deformation-basis calculations were not fine-tuned to produce as sharp a band crossing as seen in experiment, although that could have been done by slight change of deformation in the basis.) There is clearly more transfer to the yrare band over a wide range of spins for the $\beta = 0.28$ calculations than for those at smaller deformation. The corresponding histograms for the five bands of ^{158}Gd, following the ^{206}Pb two-neutron addition reaction, are shown in Fig. 6. The pattern is markedly different from Figs. 4 and 5 for ^{154}Gd in that the yrast population continues smoothly declining beyond the soft crossing around spin $18\hbar$. There is an appreciable population in the yrare band, centering around spin $20\hbar$, but the higher bands in ^{158}Gd get relatively less population than those in ^{154}Gd.

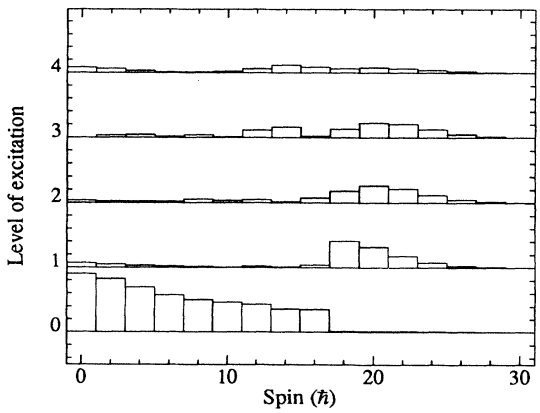

FIG. 4. Histograms show ^{154}Gd rotational bands population amplitudes from HMD-SCTDS calculation of pair extraction transfer reaction ^{206}Pb + ^{156}Gd → ^{208}Pb + ^{154}Gd. These calculations use the ^{154}Gd HMD wave functions calculated from the smaller-deformation basis single-particle levels (β=0.23). The deformed Woods-Saxon optical potential parameters used [8] were as follows: $V = 40$ MeV, $W = 40$ MeV, $r_0 = 1.2$ fm, diffuseness $a = 0.65$ fm, potential deformation parameter $\beta = 0.277$. The center-of-mass head-on collision energy of 474 MeV was chosen to give the same distance of closest approach as in the experimental conditions of Helmer *et al.* [24].

IV. COMPARISON WITH EXPERIMENT

The most comprehensive direct comparison of theory with the experimental results of Helmer *et al.* [24] is through the so-called "HK plots." In these contour plots, the horizontal axis is the number (fold) of gamma rays detected in a transfer reaction event in the 4π Oak Ridge

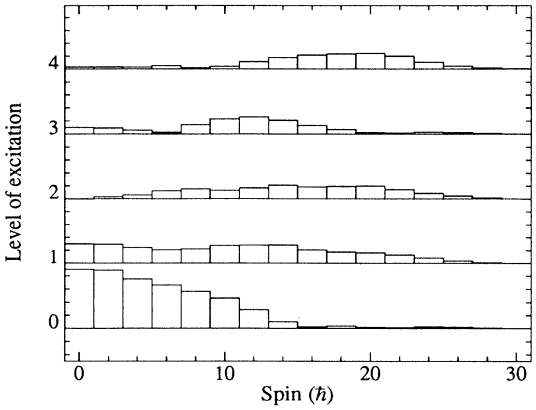

FIG. 5. Same as Fig. 4, except that the larger-deformation basis wave functions ($\beta = 0.28$) were used for the ^{154}Gd.

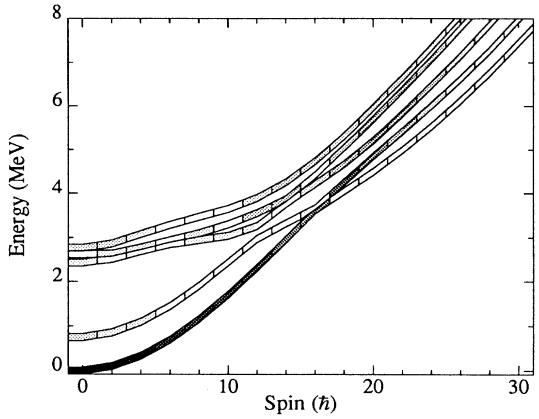

FIG. 7. Gray-scale plot of Fig. 4 for comparison to the experimental HK contour plot for ^{154}Gd, with $\beta = 0.23$ basis wave functions.

array (15 Ge and 55 NaI detectors), and the vertical axis is the sum of energies of all detected coincident gamma rays. This plot should be directly comparable with gray-scale plots of the type in Figs. 1–3. In Figs. 7 and 8 we replot the histogrammed results of Figs. 4 and 5 for ^{154}Gd as gray-scale plots, and in Fig. 9 we do the same for the histogram of Fig. 6 for transfer in the other direction to ^{158}Gd. These gray-scale plots may by qualitatively compared with the HK experimental plots (Fig. 3 of Helmer *et al.* [24]). Monte Carlo analyses of the response relating spin and fold by the experimenters for similar systems are shown in Juutinen *et al.* [25].

There is a qualitative agreement of our theory with experiment. That is, (1) the population ridge bends upward away from yrast at highest spins, showing the important roles of higher bands; (2) there is but little population to higher energy, low-spin states. Our theoretical results do not have the "rippling" of apparent peaks and saddles along the ridge, as appears notable, especially in the ^{154}Gd experimental data.

Another less direct, but more exacting, comparison

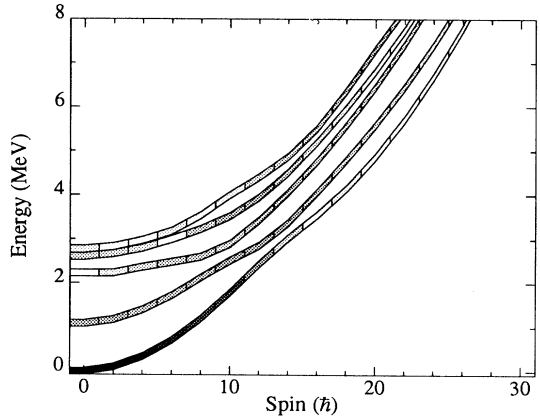

FIG. 8. Gray-scale plot of Fig. 5 for comparison to the experimental HK contour plot for ^{154}Gd with $\beta = 0.28$ basis wave functions.

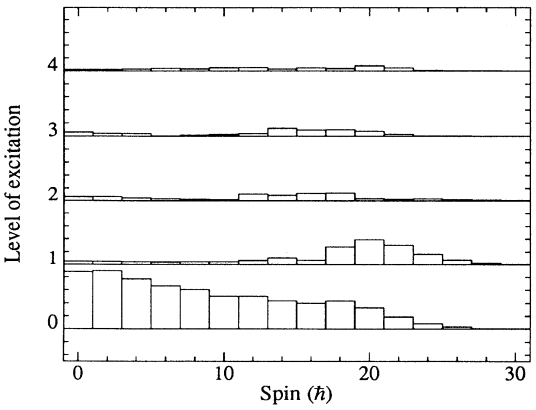

FIG. 6. Histograms show ^{158}Gd rotational bands population amplitudes from HMD-SCTDS calculation of pair deposit transfer reaction ^{206}Pb + ^{156}Gd → ^{204}Pb + ^{158}Gd.

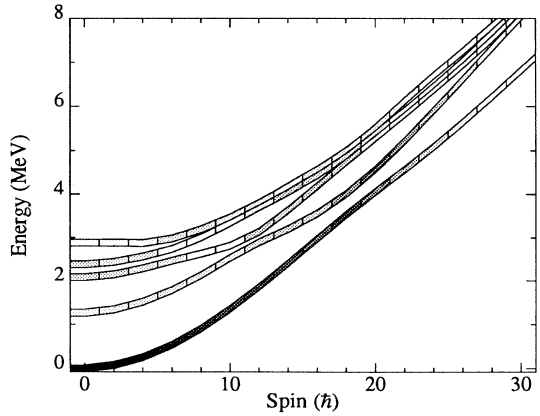

FIG. 9. Gray-scale plot of Fig. 6 for comparison to the experimental HK contour plot for ^{158}Gd.

with data is with the relative intensities of Ge-resolved yrast gamma cascade transitions. Figures 5 and 6 of Helmer *et al.* [24] make such a comparison with the theory from the simple two-band mixing model [10]. In that case there was remarkable agreement for ^{154}Gd, except for the $4 \rightarrow 2$ transition, which was 1.5 standard deviations high. There was a systematically greater falloff of theoretical gamma intensities with spin, as compared to experiment, for ^{158}Gd, although the deviations were less than two standard deviations. To make these comparisons with our present five-band theory is more complicated. We had to calculate the ~2500-term overlap functions for the $B(E2)$ values of transitions cascading down to the yrast band. We assumed only $I \rightarrow I-2$ $E2$ transitions, weighted by transition energy to the fifth power, and ignored internal conversion transitions.

The comparison for yrast gamma transitions for ^{154}Gd is shown in Fig. 10(a), plotting the new five-band theory for deformation 0.23 basis. The older two-band calculations [10] are shown in Fig. 10(b). The dashed line in Fig. 10(b) is for the diabolic case and the solid for the nondiabolic. (Recall that the diabolic point is so close to the sharp-crossing ^{154}Gd that this is an unfavorable case for testing diabolic effects. See discussions of Ref. [10].) In Fig. 10(a) we have not plotted for the larger deformation 0.28 wave functions, since they were not fine-tuned to give the sharp band crossing of experiment. Certainly the experimental HK contour plots show that we are correct in predicting excited-band population predominance for spins greater than $16\hbar$. The corresponding plot for ^{158}Gd is shown in Fig. 11. Here the five-band theory reproduces the intensity data very well, while the two-band theory of Ref. [10] falls off too rapidly, perhaps an indication of the importance of including higher bands than yrast and yrare.

V. CONCLUSIONS

It is fascinating to view the broad pattern in both the experimental HK contour plots (transfer injection point energy vs spin) and our theoretical plots with

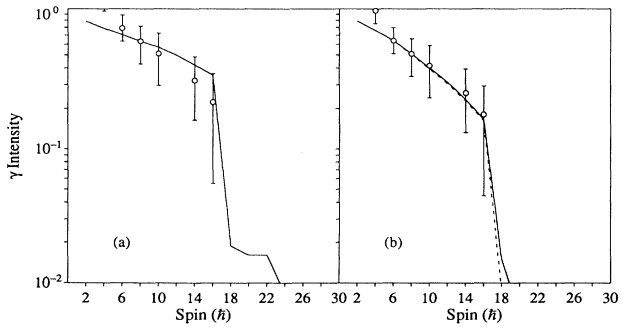

FIG. 10. Comparison with yrast gamma transition intensities for ^{154}Gd: (a) new five-band, with basis deformation 0.23; (b) old two-band calculations from Ref. [10]. Experimental data have been normalized to match theoretical results at spin 8.

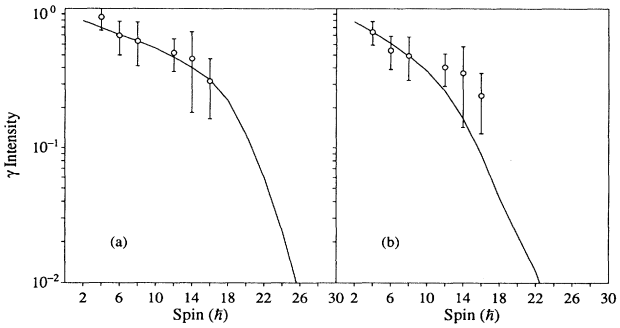

FIG. 11. Same as Fig. 8, but for ^{158}Gd.

eight bands (sudden) or five bands (time-dependent Schrödinger codes). Here we may view also our corresponding calculations on pair transfer among Dy nuclei 160, 162, and 164 [26]. The overall pattern is that the ridge of maximum pair transfer cross section lies on a parabola that rises above the yrast envelope with increasing spin. It is reasonable to associate this parabolic ridge with the fraction of the nuclear moment of inertia not due to the aligning $i_{13/2}$ orbitals, since the Coulex torque acts directly on the charged rotor core and not at all on the $i_{13/2}$ neutrons.

There is potentially other interesting microscopic information in the HK contour plots of neutron-pair transfer excitation distributions. We know from Bohr and Mottelson [27] (section 6-3f on pairing gauge transformations) about the patterns of pair transfer around closed shells. Pair-transfer strength away from the closed shell is concentrated in ground-to-ground transitions, while transfer into the closed shell as final state has substantial transfer strength split between ground and first excited state. We have observed similar patterns at neutron subshells in our calculations with thorium systems [22] with artificially bunched Nilsson neutron orbital energies. The work of Shihab-Eldin *et al.* [2] showed such patterns for (p,t) and (t,p) reactions among 0^+ states in the rare earths.

The extension of these subshell patterns to heavy-ion transfer is to be expected in that secondary ridges of population in the HK planes may appear for transfer into closed subshells of the final nucleus. Bunching of Nilsson levels further from the Fermi energy could also give rise to coherence in pair transfer and still higher-energy ridges.

Many of these generalizations about pair transfer patterns have been drawn from assumptions that pair transfer is dominated by transfer of pairs coupled to zero angular momentum. To be sure, with the usual considerations for monopole-paired BCS systems the coherence enhances $L = 0$ transfer most in ground-to-ground. However, both quadrupole pairing effects and $L > 0$ pair transfer for deformed nuclei remain an area for further exploration.

What about the question of Coriolis anti-pairing or "pairing collapse?" How are these properties manifested in the heavy-ion pair-transfer cross sections? We believe

that the progressive broadening of the parabolic ridge of transfer yield is the real measure of pairing loss. The coherent ground-state pairing strength gets fragmented onto many bands at higher spin. We do not expect, in any event, any sudden pairing collapse in nuclear systems with so few particles participating in the pairing correlation. When pairing fluctuations are folded onto the static pairing, the loss of pairing has a smooth dependence on spin. The broadening of the experimental and our five-band theoretical transfer yield parabolic ridge is indeed gradual. The aligned band strength function moves from band to band with increasing spin, eventually dominating the yrast above spin 18, and there is very little pair transfer associated with aligned-band strength.

In this paper we have taken the first steps to exploring the above effects, but there is need for continuation of formal and systematic numerical exploration that extend, as does our paper, beyond monopole pairing. Up to now the HK plot resolution of 4π gamma arrays has been limited by the low resolution of scintillation counters. With the new generations of 4π gamma arrays (EUROGAM, GAMMASPHERE, etc.) there is hope that higher-resolution data can further test, challenge, and guide theoretical calculations of the type presented here.

ACKNOWLEDGMENTS

This work was supported by the Director of Energy Research, Division of Nuclear Physics of the Office of High Energy and Nuclear Physics of the U.S. Department of Energy under Contracts DE–FG03–87ER40323, W–7405–ENG48, and DE–AC03–76SF00098. One of the authors (J.O.R.) wishes to thank the Alexander von Humboldt Foundation for support during work at the Technical University of Munich in Garching. L.F.C. and R.D. gratefully acknowledge travel support from the Brazilian-Conselho Nacional de Pesquisas e Desenvolvimento Científico (CNPq) under the U.S.-Brazil NSF-CNPq cooperative research grant INT-8382853.

[1] S. Y. Chu *et al.*, Phys. Rev. C (to be published); cf. also S. Y. Chu, Ph.D. thesis, Yale University (1993).

[2] A. A. Shihab-Eldin, J. O. Rasmussen, and M. A. Stoyer, *Microscopic Models in Nuclear Structure Physics* (World Scientific, Singapore, 1988), p. 282; cf. also A. A. Shihab-Eldin, J. O. Rasmussen, M. A. Stoyer, D. G. Burke, and P. E. Garrett, Int. J. Mod. Phys. E **4**, 411 (1995).

[3] M. W. Guidry, T. L. Nichols, R. E. Neese, J. O. Rasmussen, Z. F. Oliveira, and R. Donangelo, Nucl. Phys. **A361**, 274 (1981).

[4] J. L. Egido and J. O. Rasmussen, Phys. Rev. C **36**, 316 (1987).

[5] R. S. Nikam, P. Ring, and L. F. Canto, Z. Phys. A **324**, 241 (1986); R. S. Nikam, P. Ring, and L. F. Canto, Phys. Lett. B **185**, 269 (1987).

[6] L. F. Canto, R. Donangelo, A. R. Farhan, M. W. Guidry, J. O. Rasmussen, M. A. Stoyer, and P. Ring, in *Exotic Nuclear Spectroscopy*, edited by W. C. McHarris (Plenum Press, New York, 1990), p. 625.

[7] L. F. Canto, R. Donangelo, M. W. Guidry, A. R. Farhan, J. O. Rasmussen, P. Ring, and M. A. Stoyer, Phys. Lett. B **241**, 295 (1990).

[8] L. F. Canto, R. Donangelo, J. O. Rasmussen, P. Ring, and M. A. Stoyer, Phys. Lett. B **248**, 10 (1990).

[9] C. H. Dasso and A. Winther, Phys. Lett. B **242**, 323 (1990).

[10] L. F. Canto, P. Ring, Y. Sun, J. O. Rasmussen, S. Y. Chu, and M. A. Stoyer, Phys. Rev. C **47**, 2836 (1993).

[11] K. Alder and A. Winther, *Coulomb Excitation* (Academic Press, New York, 1966), cf. appendix on deBoer Winther computer code, p. 303.

[12] I. S. Towner and J. C. Hardy, Adv. Phys. **18**, 401 (1969).

[13] U. Götz, M. Ichimura, R. A. Broglia, and A. Winther, Phys. Lett. **16**, 115 (1975).

[14] W. Von Oertzen, Phys. Rev. C **43**, R1522 (1991).

[15] J. Speer *et al.*, Phys. Lett. B **259**, 422 (1991).

[16] R. Künkel *et al.*, Phys. Lett. B **208**, 355 (1988).

[17] W. Von Oertzen, G. Bohlen, B. Gebauer, R. Künkel, F. Pühlhofer, and D. Schüll, Z. Phys. A **326**, 463 (1987). A very detailed look at the contributions of different shell-model configurations in the $1n$ intermediate state is given in Table 3 for Sn-Sn collisions.

[18] D. H. Feng, T. Udagawa, and T. Tamura, Nucl. Phys. **A274**, 262 (1976).

[19] R. A. Broglia and Aa. Winther, *Heavy Ion Reactions*, Parts 1 and 2 (Addison-Wesley, Redwood City, CA, 1990).

[20] P. Lotti, A. Vitturi, R. A. Broglia, and Aa. Winther, Nucl. Phys. **A254**, 95 (1991).

[21] C. H. Dasso and S. Landowne, Z. Phys. A **322**, 175 (1985). Also C. H. Dasso, S. Landowne, R. Broglia, and Aa. Winther, Phys. Lett. **73B**, 401 (1978).

[22] S. Y. Chu, J. O. Rasmussen, R. Donangelo, M. A. Stoyer, S. Frauendorf, and Y. R. Shimizu, in *Proceedings of the Conference on Nuclear Physics in Our Times, Sanibel Island, Florida, 1992*, edited by A. V. Ramayya (World Scientific, Singapore, 1993), p. 181.

[23] K. Alder and A. Winther, *Electromagnetic Excitation* (North-Holland, Amsterdam, 1975).

[24] K. G. Helmer, C. Y. Wu, D. Cline, A. E. Kaavka, M. W. Guidry, X. L. Han, R. W. Kincaid, X. T. Liu, J. O. Rasmussen, A. Shihab-Eldin, and M. A. Stoyer, Phys. Rev. C **48**, 1879 (1993).

[25] S. Juutinen, X. T. Liu, S. Sorensen, B. Cox, R. W. Kincaid, C. R. Bingham, M. W. Guidry, W. J. Kernan, C. Y. Wu, E. Vogt, T. Czosnyka, D. Cline, M. L. Halbert, I. Y. Lee, and C. Baktash, Phys. Lett. B **192**, 307 (1987).

[26] J. O. Rasmussen, L. F. Canto, S. Y. Chu, R. Donangelo, and M. A. Stoyer, Proceedings of the Conference on Harmony in Physics, honoring Belyaev 70th birthday, University of Pennsylvania, Philadelphia, 1994 [Phys. Rep. (to be published)].

[27] A. Bohr and B. R. Mottelson, *Nuclear Structure*, Vol. 2 (Benjamin, Reading, MA, 1975).